Introduction of the Optimal Cloud Analysis for Himawari-8/-9

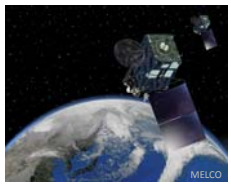

Himawari-8/-9

Masahiro Hayashi*

*The Meteorological Satellite Center of the Japan Meteorological Agency

masa_hayashi@met.kishou.go.jp

Introduction

The Japan Meteorological Agency (JMA) plans to launch the next-generational satellite "Himawari-8" in summer 2014 and commence its operation in 2015 (Figure 1). The Advanced Himawari Imager (AHI) on board Himawari-8/-9 will have 16 bands from visible to infrared range (3 visible, 3 near infrared and 10 infrared bands). For the maximum utilization of AHI, JMA has been working on implementation of the Optimal Cloud Analysis (OCA) developed by EUMETSAT (EUMETSAT 2011) with EUMETSAT kind cooperation since last year.

OCA adapts the optimal estimation method to retrieve cloud parameters (e.g. cloud optical thickness, cloud effective radius, cloud top pressure and surface temperature). Since different AHI bands have different sensitivity to the parameters, high-qualified cloud parameters are expected by applying the optimal estimation method to the multiband data with AHI. In addition to the increased bands, temporal resolution of observation will be enhanced on Himawari-8. Cloud parameter retrieval with high-frequency imageries will provide additional information on evolution of cloud systems.

JMA plans to utilize cloud top heights derived from OCA which can treat 2-layer clouds (Watts et al. 2011) to Atmospheric Motion Vector products (AMVs). Multi-layer clouds that are common on the application to the satellite remote sensing make AMVs height assignment (HA) accuracy degraded. Optimal utilization of multi-layered cloud top height to AMV HA algorithm is under investigation at JMA.

Himawari-8/-9 Imager bands (AHI)

Wavelength (μm)	Himawari-8/9		MTSAT-1R/2		GOES-R		MSG	MTG
0.46	●	1			●	1		●
0.51	●	1						●
0.64	●	0.5	●	1	●	0.5	●	●
0.86	●	1			●	1	●	●
0.96								●
1.3					●	2		●
1.6	●				●	1	●	●
2.3	●				●			●
3.9	●		●		●		●	●
6.2	●		●		●		●	●
7	●	2		4	●			
7.3	●				●		●	●
8.6	●				●	2	●	●
9.6	●				●		●	●
10.4	●		●		●		●	●
11.2	●				●			
12.3	●		●		●		●	●
13.3	●	km		km	●	km	●	●

A sequence of AHI observation in 10 minutes time frame

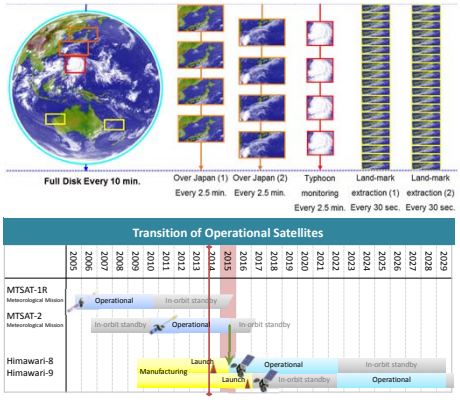

Fig. 1 Schedule and Specification of Himawari-8/9

Methodology

OCA estimates cloud physical properties ($\boldsymbol{x}$) with multi-channel radiances $\boldsymbol{y}_m$ (from visible to infrared wavelength) by the 1D-VAR method.

In this method, following cost function will be minimized:

$$J = (\boldsymbol{y}_m - f(\boldsymbol{x}))^T S_y^{-1} (\boldsymbol{y}_m - f(\boldsymbol{x})) + (\boldsymbol{x} - \boldsymbol{x}_a)^T S_x^{-1} (\boldsymbol{x} - \boldsymbol{x}_a)$$

The cost function is minimized by the Levenburg-Marquardt Descent

$$\delta \boldsymbol{x} = -\left(\frac{\partial^2 J}{\partial \boldsymbol{x}^2} + \alpha \boldsymbol{I}\right)^{-1} \frac{\partial J}{\partial \boldsymbol{x}}$$

S: error covariance matrix
$\boldsymbol{x}_a$: a priori state vector

$\boldsymbol{x}$ = Cloud Effective Radius, Cloud Optical Thickness, Cloud Fraction, Cloud Top Pressure, Surface Temperature

The forward model $f(\boldsymbol{x})$ is divided by two wavelength range :

Short Wave Radiation (visible to near-infrared)

$$f(\boldsymbol{x}) = T_{2ac}\rho_{BD} + \frac{T_{2ac} T_B T_D \rho_S}{1 - T_{2bc}\rho_D \rho_S}$$

Clear sky atmospheric transmission (T_{2ac}, T_{2bc})
→ fast radiative calculation with NWP model (RTTOV11 Hocking et al. 2013)
Cloud reflection (ρ_{BD}, ρ_D) and transmission (T_B, T_D)
→pre-calculated LUT (DISORT Stemnes et al. 1988)
Surface BRDF (ρ_S)
→Land: climatology (MODIS BRDF Luchet et al. 2006), Sea: Cox & Munk 1954

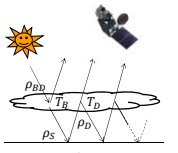

Long Wave Radiation (infrared)

$$f(\boldsymbol{x}) = R_{bc} T_D T_{ac} + B(T)\varepsilon_c T_{ac} + R_{ac}^{\downarrow} \rho_D T_{ac} + R_{ac}$$

Clear sky atmospheric transmission (T_{ac}, T_{bc}) and radiation (R_{ac}, $R_{ac}^{\downarrow}$)
→ fast radiative calculation with NWP model (RTTOV11)
Cloud reflection (ρ_D), emissivity (ε_c) and transmission (T_D))
→pre-calculated LUT (DISORT)
Radiance below the cloud (R_{bc})
→NWP model, OCA parameter (surface temperature) and surface emissivity (Land: climatology Seemann et al. 2008, Sea : Masuda 2006)

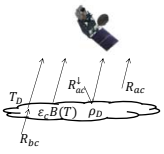

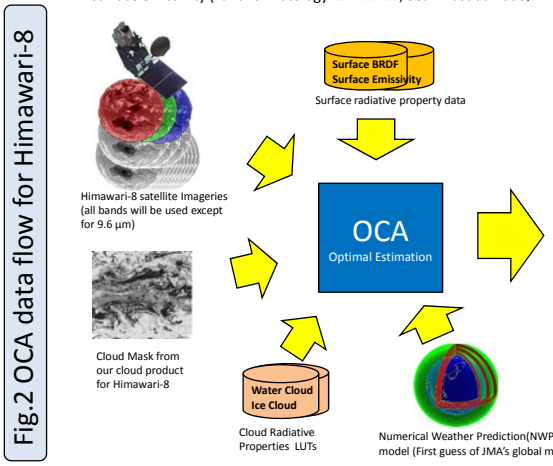

Fig.2 OCA data flow for Himawari-8

Results

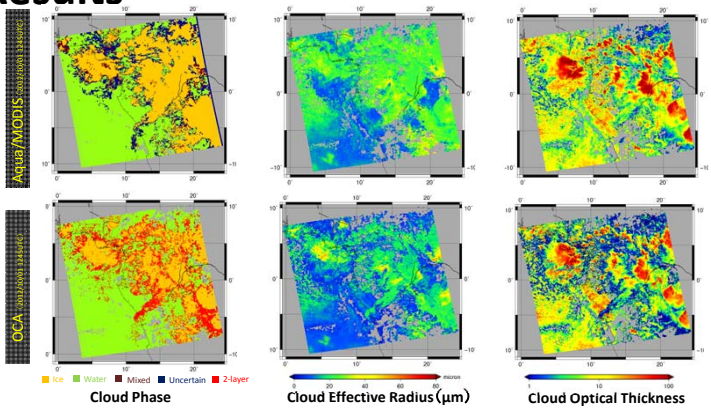

Fig. 3 Comparison with MODIS products (OCA is from SEVIRI Ch1~Ch11 and JMA's NWP model is used)

Calipso 523 nm total backscatter

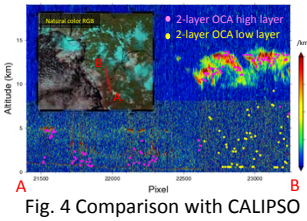

Fig. 4 Comparison with CALIPSO

Currently JMA runs the OCA with SEVIRI data as proxy of AHI data. The output cloud parameters by OCA were compared with MODIS Level-2 cloud products and CALIPSO products at JMA. Figure 3 displays a comparison between MODIS and OCA outputs (01/10/2012 1245UTC). Cloud phase are well correlated except for ice-cloud edges where anvils from cumulonimbus clouds dominate (uncertain and 2-lyaer on the figure). MODIS and OCA cloud effective radius are similar except for the anvil area. Also cloud optical thickness are similar except for the area on which values are smaller because of thin upper cirrus.

Figure 4 shows matchup between OCA cloud top height and CALIPSO 523 nm total attenuated backscatter on the same scene as Figure 3. 2-layer clouds are detected on "B" side and some water clouds are assigned as 1-layer on "A" side. Between these 1-layer water clouds, lower clouds are not detected in the cloud mask procedure, therefore cloud top heights are not assigned.

Discussion

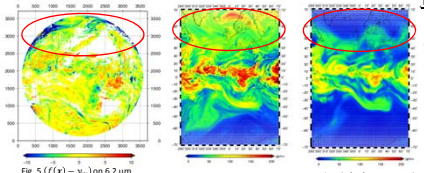

Fig. 5 $(f(\boldsymbol{x}) - \boldsymbol{y}_m)$ on 6.2 μm (1/10/2012 12 UTC) Bias correction (+4K)

Fig. 6 Water vapor mixing ratio at 200 hPa (1/10/2012 12 UTC) Left: JMA's global model (First guess) Right: ERA-Interim

The NWP model forecast error

OCA implemented in JMA has relatively large $f(\boldsymbol{x}) - \boldsymbol{y}_m$ biases on the water-vapor channel (Figure 5. Except for 6.2 μm, there are small biases) . The investigation to reveal what causes the bias was executed. As one approach to realize this problem, the NWP model dependency on the forward model was analyzed. ERA-Interim and upper sounding data was used to estimate the impact of model error. Figure 6 describes 200 hPa water vapor-mixing ratio of JMA NWP model and ERA-interim.

Figure 7 shows difference between SEVIRI 6.2μm and simulated clear sky brightness temperature (BT) using RTTOV11 at 1/10/2012 12 UTC. It shows that the BT simulated from JMA's global model has the bias about 4 K in average, while the one from ERA-Interim data has small biases.

These facts indicate that the bias was caused by high-amount of water vapor in the upper atmosphere (especially seen inside the red circles on the figures). Clear-sky transmittance from upper troposphere calculated from vertical profiles of the sounding data support the results of the discrepancy of the model (not shown). Some methods to correct water vapor profiles might be required to obtain more accurate cloud retrieval parameters especially for height assignment.

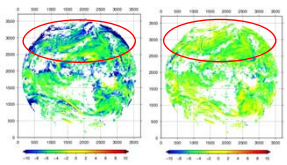

Fig. 7 Difference between SEVIRI 6.2μm and simulated clear-sky-brightness temperature (B-O, 1/10/2012 12 UTC) Left: JMA's global model Right: ERA-Interim

New ice single-scattering property database for Himawari-8

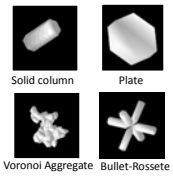

Fig.8 Various types of Ice crystals treating at MRI/JMA (Ishimoto et al. 2012)

Currently JMA OCA uses radiative property Look Up Tables (LUTs) provided by EUMETSAT for SEVIRI. To prepare LUTs of ice cloud radiative property for AHI, the Meteorological Research Institute (MRI) of JMA is calculating single-scattering radiative properties with the methods of FDTD , improved geometric optics (GOM2) and geometric optics (GOM) (Ishimoto et al. 2012) for AHI spectral response functions. Scattering properties (e.g. size-averaged single scattering albedo and phase function) which drive the multi-scattering radiative transfer model are calculated from the ice-scattering database. Meanwhile, water cloud scattering properties are calculated with the Lorenz-Mie theory of scattering.

It is planned to adapt appropriate ice habits to represents ice clouds after sensitivity experiment of the various ice shapes (at first solid column and Voronoi aggregation will be used for convenience) .

Acknowledgements

This work is greatly assisted by EUMETSAT. I am really grateful to Philip Watts for kind advices and providing many materials of OCA. I thank to MRI/JMA for providing sea surface emissivity calculation code and scattering database for this work.

Reference

Cox C. and W. Munk, 1954: Measurement of the roughness of the sea surface from photographs of the sun's glitter. *J. Opt. Soc. Am.* **44**, 838-850

EUMETSAT, 2011: ATBD for Optimal Cloud Analysis Product. EUMETSAT

Ishimoto H., K. Masuda, Y. Mano, N. Orikasa and A. Uchiyama, 2012: Irregularly shaped ice aggregates in optical modeling of convectively generated ice clouds. *JQSRT*, **113**, 632-643

Hocking, J, P. Rayer, D. Rundle, R. Saunders, M. Matricardi, A. Geer, P. Brunel and J. Vidot, 2013: RTTOV v11 users guide. *NWP SAF*

Lucht W., C. B. Schaaf and A. H. Strahler, 2000: An algorithm for the retrieval of albedo from space using semiempirical BRDF models. *IEEE Trans. Geo. And Rem. Sen.*, **38**, 977-998

Masuda K., 2006: Infrared sea surface emissivity including multiple reflection effect for isotropic Gaussian slope distribution model, *Rem. Sen. Env.*, **103**, 488-496

Seemann W. S., E. E. Borbas, R. O. Knuteson, G. R. Stephenson and H.-L. Huang, 2008: Development of a Global Infrared Land Surface Emissivity Database. *J. Appl. Meteor.*, **47**, 108-123

Stemnes K., S.-C. Tsay, W Wiscombe and K. Jayaweera, 1988: Numerically Stable Algorithm for Discrete-Ordinate-Method Radiative Transfer in Multiple Scattering and Emitting Layered Media, *App. Opt*, **27**, 2502-2509

Watts, P. D., C. T. Mutlow, A. J. Baran, and A. M. Zavody 1998: Study on Cloud Properties Derived from Meteosat Second Generation Observation. *EUMETSAT*

Watts P. D., R. Bennartz and F. Fell, 2011: Retrieval of Two-layer Properties from Multispectral Observations Using Optimal Estimation. *J. Geophys. Res.*, **116**, D16203